

To Design a CFD Model Optimizing a Co- Designed Microfluidic Chip with Manifold Micro Channels

Bablu Singh

Department of Chemical Engineering, Indian Institute of Technology
Guwahati, Assam, India, 781039

Guide: Prof. Raghvendra Gupta

Department of Chemical Engineering, Indian Institute of Technology
Guwahati, Assam, India, 781039

Mentor: Sanjay Ramachandran

FOSSEE IIT Bombay

Abstract

The objective of this study is to investigate the microchannel cooling for microelectronic in microfluid channel by passing coolant liquid. The system operates on the principle of conjugate heat transfer, simultaneously solving the fluid flow and heat conduction in both liquid and solid regions. Numerical simulations were employed to optimize the module's geometric design. The study primarily focuses on the influence of channel boundaries and liquid- solid interactions on flow patterns. The study investigates the effects of varying flow conditions 1 mm/s and 10 mm/s, represented by the inlet velocity.

1. Introduction

1.1 Background

The rise in chip power and assembly density has made cooling a crucial factor in the design and operation of modern data centres (DCs). Microelectronic devices are now a crucial part of all military and civil equipment and have contributed significantly to technological advancement. Their growth rate has increased significantly since their yearly use has increased noticeably. Microelectronic device shrinkage has become a common feature and a gauge of product development and quality over the past two decades.

Alongside this, there are now fewer spaces available for heat-dissipation systems. The rising density of electronic components in a shrinking footprint result in an exponential increase in power density, which produces vast amounts of heat. If this heat is not efficiently dissipated, it can result in system performance degradation, loss of reliability, and even system failure. At the microscale, the drawbacks of conventional cooling techniques are clearly visible. While they work well for larger systems, conventional methods such as heat sinks with forced air convection become less efficient as the device gets smaller. A more advanced and localised approach to thermal management is required due to the physical limitations and the high heat flux produced by microelectronic devices. The discipline of microfluidics presents a viable remedy in this regard. Microfluidic accurately manage microscopic quantities of liquids and gases makes it particularly suited for localized heat removal. By employing micro-channels to guide a cooling fluid directly to the heat source, microfluidics facilitates the creation of highly efficient heat transfer systems within thermal management. Compared to conventional techniques, this allows for far more intimate thermal coupling between the cooling fluid and electronic components, resulting in better heat dissipation.

Using manifold micro-channels is one of the best ways to apply microfluidic cooling. These complex channels, which are frequently built right into the electronic device's substrate or a special cooling plate, offer a lot of surface area for heat exchange in a very small package. The device is kept at its ideal operating temperature by the fluid that passes through these micro-channels, which removes heat. Significant benefits of this method include a small form factor, a high capacity for heat removal, and the possibility of heterogeneous integration with the electronic components.

Microfluidic cooling systems have their own set of difficulties in terms of design and optimisation, despite their potential. In-depth knowledge and advanced modelling are necessary to fully comprehend the intricate fluid dynamics at the microscale, which include phenomena like surface tension effects and laminar flow. Here, computational fluid dynamics, or CFD, has emerged as an important tool that helps engineers simulate heat transfer and fluid flow within microchannels, which they can then design to ensure highest efficiency. Conclusion: To surpass the thermal limitations to further miniaturisation and realise the full potential of next-generation electronic systems, it is essential to create more sophisticated thermal management technologies, particularly those utilising microfluidics and CFD.

1.2 Relevance in Natural and Engineering Applications

Microfluidic use in biomedical applications is one of its most significant applications. Microfluidic devices, often referred to as "lab-on-a-chip" systems, can perform complex laboratory work on a single miniature chip. Microfluidic devices analyse small blood or saliva samples for speed diagnostics, such as point-of-care disease testing. They are also critical in drug discovery and development since they provide a means for high-throughput screening of potential drug candidates as well as the creation of organ-on-a-chip models that better mimic human physiology than traditional cell cultures. Microfluidics is ideal for these purposes due to its precision and minimal sample volume demand.

In addition, thermal management, particularly for electronics, is being transformed by microfluidics. Cooling heat becomes an ever-growing challenge as electronic components become more powerful and compact. Microfluidic cooling systems are offering an extremely effective solution in which they flow a coolant directly over the heat source through networks of microchannels. As described earlier when dealing with data centres and supercomputers, this is required for the reliable operation of high-performance microprocessors, LEDs, and other heat-sensitive devices.

Environmental science and chemical engineering are among the areas where microfluidics is also making significant progress. Chemical applications are made safer and offer better yields for reactions by controlling reaction conditions, including temperature and concentration of reactants, with nanometre accuracy, courtesy of microfluidic reactors. This is particularly useful in generating new materials or performing dangerous reactions

on a small but controlled scale. Microfluidic sensors in environmental monitoring can easily and sensitively detect poisons or contaminants in water samples. The small size of such devices also renders them suitable for in-situ measurement in remote or hard-to-reach regions.

2. Problem Statement

A conjugate heat transfer schematic diagram can be simplified in the in figure 2.1. The computational domain is a 0.1 m x 0.1 m rectangular box with two parallel walls and two open ends that act as a liquid's inlet and outlet. As a heating source, a central rectangular block that is 0.025 m by 0.015 m is placed inside the enclosure. Analysing the heat transfer and fluid flow properties in this configuration is the simulation's goal. The velocity contour shows the liquid flows around the obstruction, impacted by both the inflow flow and natural convection brought on by the temperature gradients, the temperature contour depicts a confined hot area surrounding the source. This configuration analyses the forced and mixed convection, where heat effects and fluid dynamics are closely related. Because both forced and natural convection mechanisms are involved, the simulation explores a mixed convection regime. The flow velocity, fluid characteristics, and the magnitude and power of the heat source all affect how dominant one is over the other.

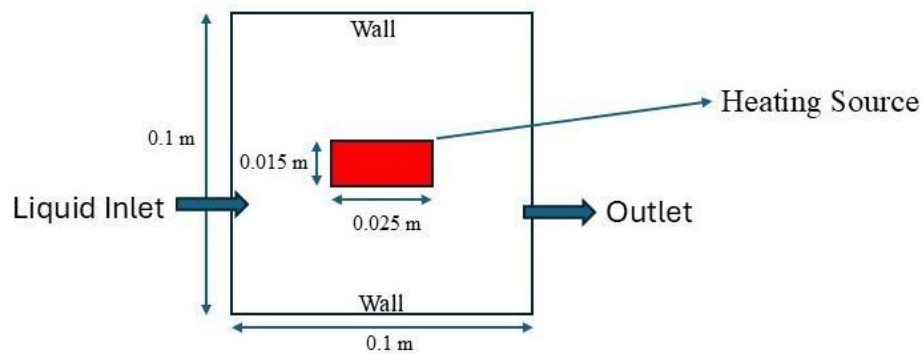


Figure 0.1: Schematic diagram of control volume to simulate the heat transfer

3. Governing Equations

The fluid flow is modelled by continuity and Navier-Stokes equations. The fluid is assumed to be Newtonian and incompressible. The Navier-Stokes equations regulate the flow.

$$\frac{\partial \rho_f \bar{u}_i}{\partial x_i} = 0 \quad (3.1)$$

$$\frac{\bar{u}_j \rho_f \bar{\partial u}_i}{\partial x_j} - \frac{\partial p}{\partial x_i} + \frac{\partial}{\partial x_j} [(\mu + \mu_t) (\frac{\bar{\partial u}_j}{\partial x_i} + \frac{\bar{\partial u}_i}{\partial x_j})] \quad (3.2)$$

Convection-Diffusion Equation, specifically describing the transport of temperature in a fluid, accounting for both convective transport by mean velocity and diffusive transport due to molecular and turbulent effects.

$$\frac{\bar{u}_j \rho_f \bar{\partial T}}{\partial x_j} = \frac{\partial}{\partial x_j} [(\frac{\mu_l}{\sigma_l} + \frac{\mu_t}{\sigma_t}) \frac{\partial T}{\partial x_j}] \quad (3.3)$$

$$\frac{\partial}{\partial x_i} [k_s \frac{\partial T}{\partial x_i}] = 0 \quad (3.4)$$

The coupling is completed at the interface between the fluid and solid regions. At the boundary, the temperature and heat flux are matched, ensuring a smooth and physically realistic transfer of heat from one domain to the other.

4. Simulation Procedure

4.1 Geometry and Mesh

The computational mesh has been generated using the blockMesh utility, with the geometry defined in the blockMeshDict file. A global scaling factor of convertToMeters 0.1 is applied, giving the channel dimensions as $0.2 \text{ m} \times 0.2 \text{ m} \times 0.01 \text{ m}$ in the x, y, and z directions respectively. The mesh consists of a single hexahedral block defined by eight vertices, discretized into $1000 \times 1000 \times 1$ cells along the x, y, and z directions, resulting in a total of 1,000,000 cells. This fine resolution in the x–y plane ensures accurate capture of flow and temperature gradients within the microchannel, while the single cell in the z-direction imposes a quasi-2D nature to reduce computational cost. The boundary patches are defined as follows: the inlet and outlet are modeled as patches to allow fluid entry and exit, the fixedWalls represent the channel’s solid walls treated as no-slip boundaries, and the frontAndBack faces are specified as empty to enforce two-dimensional behaviour. This setup provides an efficient yet accurate mesh for simulating laminar microfluidic cooling flows.

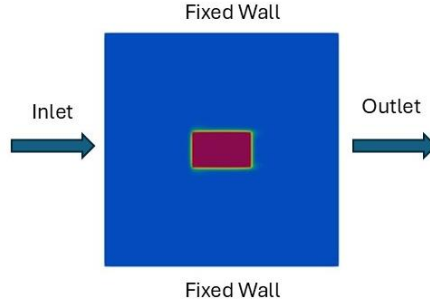


Figure 0.1: Geometry of the simulation domain

4.2 Initial and Boundary Conditions

The coupling present in chtMultiRegionFoam is conjugate heat transfer (CHT). Heat transfer is simultaneously solved in the fluid and solid domains in this multiphysics connection. An incompressible turbulent fluid flows based on the fluid dynamics equations. Although the Reynolds-Averaged Navier-Stokes (RANS) momentum equation, which governs the fluid velocity and pressure, is equation 3.2, equation 3.1 provides for mass conservation. The turbulent viscosity term indicates that turbulent flow phenomena are accounted for in this formulation, which is of significance in making accurate heat transfer calculations.

Second, temperature variations in both the fluid and solid domains are described by the heat transfer equations (3.3 and 3.4). The fluid's Convection-Diffusion equation is found in Equation 3.3. The fluid's velocity field, which is determined by the momentum equation (3.2), directly affects its convective term. This link is essential because it demonstrates how thermal energy is physically transported by the fluid's velocity. This equation's diffusion term also incorporates turbulent effects, suggesting that heat transmission is improved by chaotic fluid motion.

4.3 Solver

The solver `chtMultiRegionFoam` has been selected to solve the present case as it allows the coupled simulation of heat conduction in solids and heat convection in the fluid region. This makes it particularly suitable for microfluidic cooling problems where conjugate heat transfer plays a significant role. Another important criterion for the selection of this solver is its ability to model transient behaviour, since the equations solved by `chtMultiRegionFoam` are inherently time dependent.

In addition, when conjugate heat transfer is considered, separate regions for the solid and fluid domains must be defined, and their thermal interaction is handled at the region interfaces. The solver requires initialization of additional thermophysical parameters for both solid and fluid regions, as it simultaneously solves the energy equation in the fluid and the heat conduction equation in the solid. As the operating Reynolds number lies in the low-Re regime, the simulation type has been set to laminar across the entire fluid domain. The Courant–Friedrichs–Lewy (CFL) condition has also been maintained to ensure numerical stability; for the present unsteady simulation, the CFL number was restricted below 1, resulting in a chosen time step (Δt) appropriate for stable and accurate transient resolution.

5. Results and Discussion

5.1 Numerical Validation

The present numerical method, `chtMultiRegionFoam` with a laminar flow assumption, is a well-established and validated approach for simulating conjugate heat transfer problems. The accuracy of the method is demonstrated through a test case involving the flow and heat transfer of a fluid around a heated solid obstacle within a confined channel. This specific scenario is used to validate the solver's capability in accurately predicting the complex interplay between fluid dynamics and thermal energy transport, particularly under conditions of mixed convection. The simulation results for key parameters, such as the temperature and velocity distributions, are compared against established numerical data and experimental measurements from existing literature, confirming the method's reliability for modelling these coupled phenomena.

The problem's schematic diagram is like the setup described in Figure 3.1, where a solid block is cantered within a channel. In this case, the channel width is specified relative to the characteristic dimension of the heated block, such as its height. A key aspect of this test case is the geometric ratio of the block's dimensions, which, along with fluid properties and flow conditions, dictates the thermal and fluid dynamic behaviour, including the relative dominance of forced versus natural convection. The simulation aims to accurately capture these complex heat transfer phenomena and validate the solver's predictions against test case presented by Deng et al. (2023).

5.2 Influence of Geometry on Thermal Field

Temperature distribution along the x-axis passing through the heated block. This plot provides a quantitative analysis of the simulation results for two different inlet velocities: 10 mm/s and 1 mm/s. The lower velocity (1 mm/s) of coolant liquid, shows a significant temperature increase and a peak temperature of approximately 328 K. This is

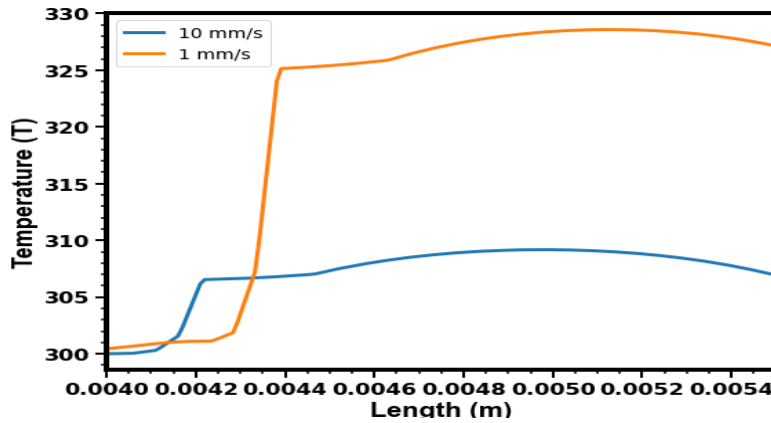


Figure 0.1: Temperature distribution along the x-axis passing through the centre of the heat sink.

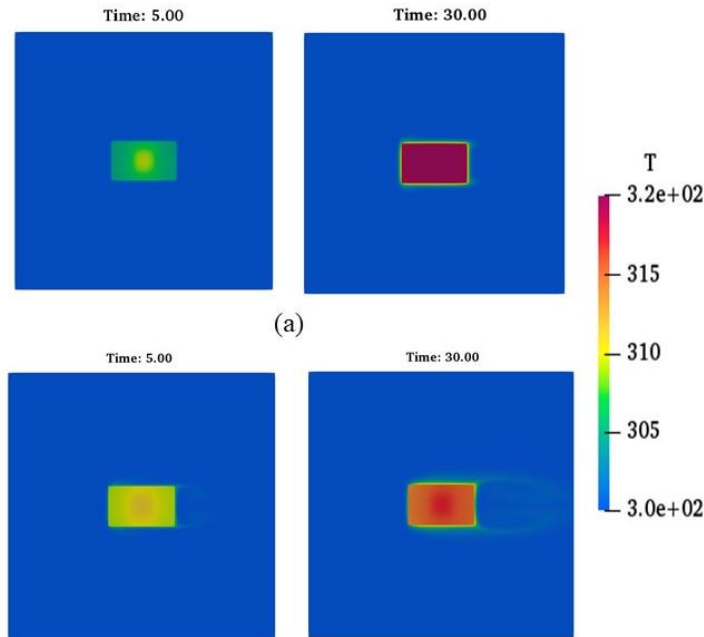


Figure 0.2: Temperature contours (a) at 1mm/s of liquid inlet velocity and (b) 10mm/s liquid inlet velocity

because the slower-moving fluid has more time to absorb heat from the block, resulting in a less efficient cooling effect. Conversely, for the higher velocity (10 mm/s) shows a much smaller temperature rise and a lower peak temperature of about 309 K. This demonstrates

that a higher flow rate enhances convective cooling by more effectively transporting thermal energy away from the heat source.

At 1 mm/s (top row) the flow is slower, so the heat plume develops more vertically and is less stretched downstream. At $t=5s$, the plume is small and localized. By $t=30s$, the plume has grown significantly, and the temperature within it is much higher. The slower flow allows for a greater temperature build-up in the fluid, resulting in a more pronounced and vertically dominant heat plume. At 10 mm/s (bottom row) the flow is faster, so the heat plume is more stretched horizontally in the direction of the flow. At $t=5s$, a clear downstream thermal wake is already visible, indicating the rapid transport of heat. By $t=30s$, the plume is elongated and less intense in terms of peak temperature compared to the 1 mm/s case. This demonstrates that the velocity of the forced flow directly controls the shape, size, and temperature of the heat plume, with higher velocities leading to longer, less concentrated plumes and more effective cooling.

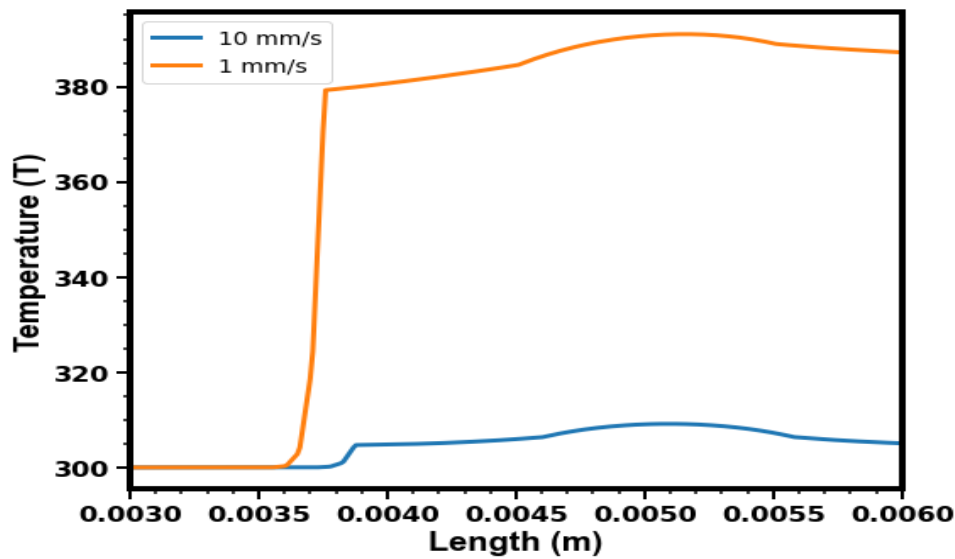


Figure 0.3: Temperature distribution along the y-axis passing through the centre of the heat sink.

As the cooler fluid approaches the heated block, a thin layer of fluid directly adjacent to the solid surface begins to heat up. This is a region dominated by molecular diffusion of heat. The steepness of the temperature curve at this point indicates a high temperature gradient, which, according to Fourier's Law of Heat Conduction, implies a high heat flux from the solid to the fluid. At the higher velocity (10 mm/s), the flow is more vigorous, which thins both the thermal and velocity boundary layers. This thin boundary

layer enhances the temperature gradient and heat transfer coefficient, leading to more efficient cooling and a lower peak temperature.

5.3 Effect of Geometry on Flow Velocity

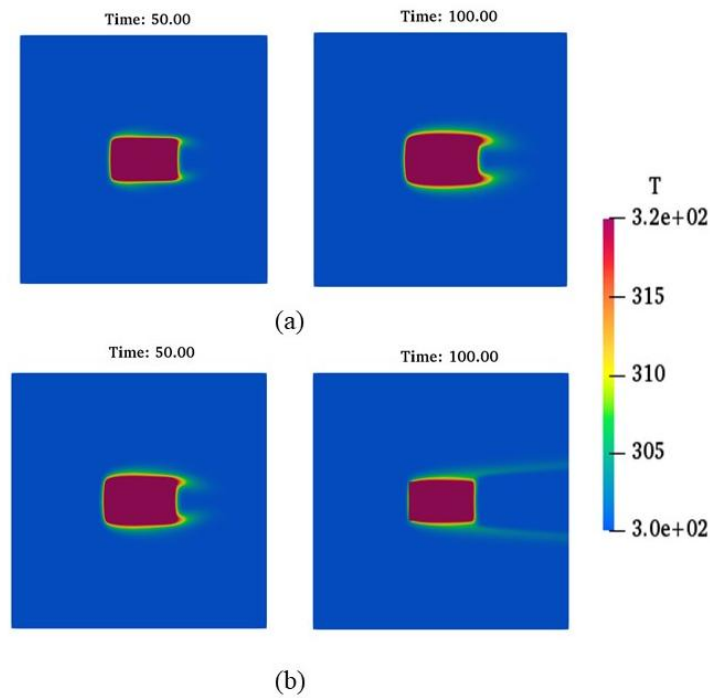


Figure 0.4: Temperature contours (a) at 1mm/s of liquid inlet velocity and (b) 10mm/s liquid inlet velocity at time $t= 50s$ and $100s$

Figure 4.5 (a) shows the velocity profile for a 1 mm/s inlet velocity. The velocity starts near zero at the wall, increases to the inlet velocity, and then accelerates to a peak value greater than 1 mm/s as it is forced to flow through the narrow gap around the heated block. After passing the block, the velocity gradually returns to a more uniform state. Figure 4.5 (b) shows the same behaviour for a 10 mm/s inlet velocity. The peak velocity is now significantly higher, reflecting the greater momentum of the flow. at the lower velocity (1 mm/s), the boundary layer is thicker, which reduces the temperature gradient at the surface and hinders the rate of heat removal, resulting in a higher surface temperature. The interplay between forced convection (driven by the inlet velocity) and natural convection (driven by buoyancy) determines the overall flow and temperature field. This interaction can be quantified by the ratio of the Grashof number (Gr) to the square of the Reynolds number (Re). As $Gr/Re \ll 1$, forced convection dominates, if $Gr/Re \gg 1$, natural convection dominates and if $Gr/Re \approx 1$, both are equally important (mixed convection).

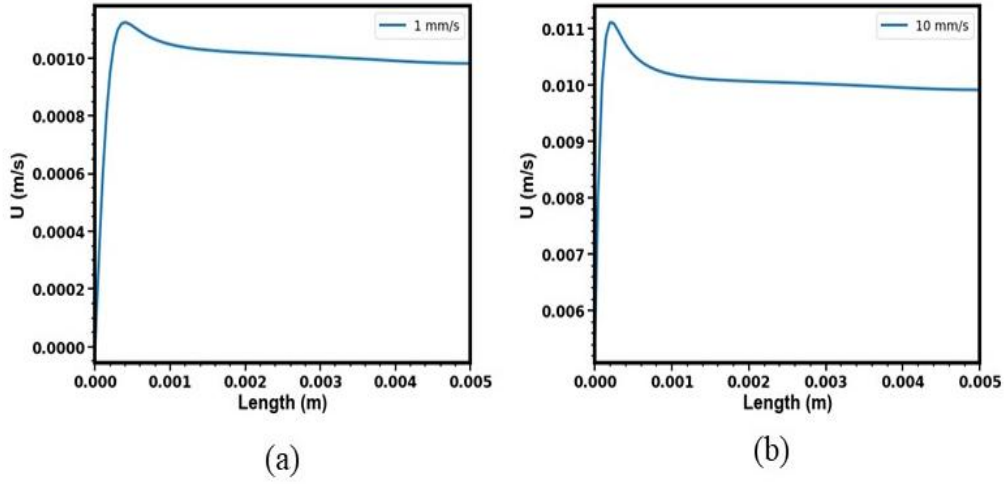


Figure 0.6: Velocity profiles along the channel for inlet velocities of 1 mm/s (a) and 10 mm/s (b).

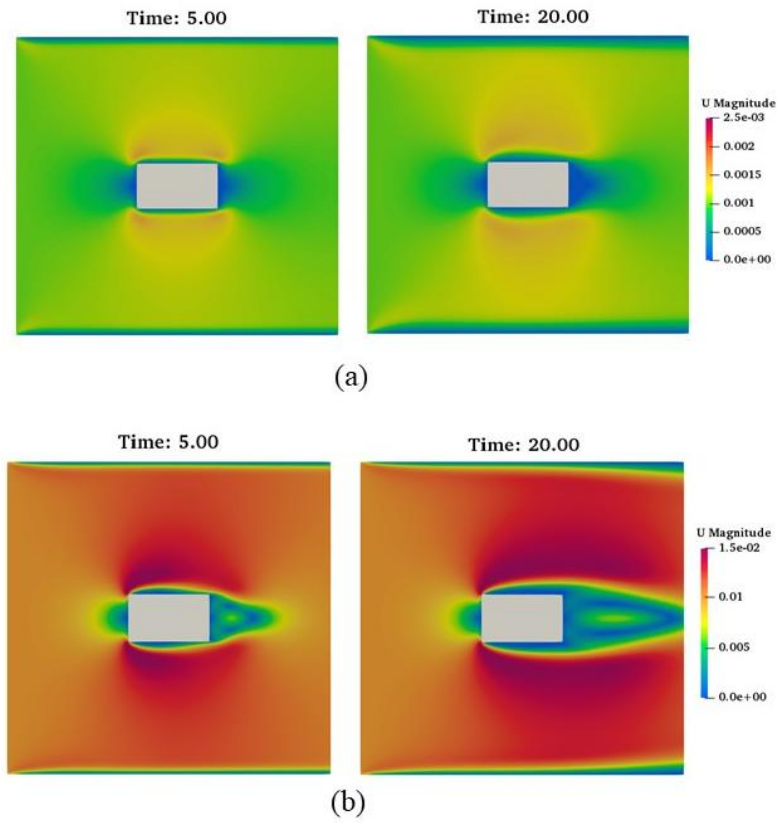


Figure 0.5: Velocity contour plot showing the fluid flow patterns around the heated block at different time for (a) 1mm/s and (b) 10 mm/s at $t = 5$ s and 20 s

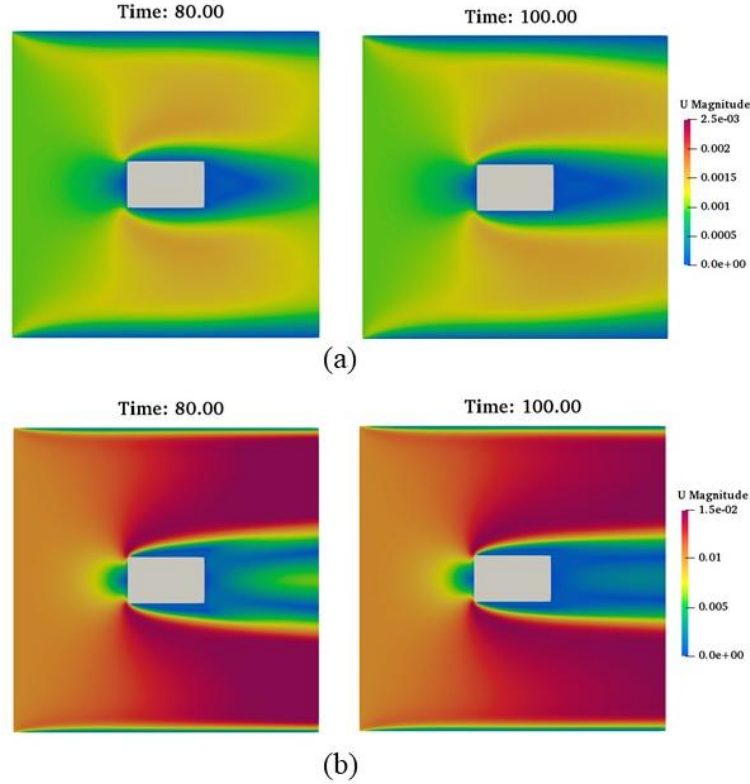


Figure 0.7: Velocity contour plot showing the fluid flow patterns around the heated block at different time for (a) 1mm/s and (b) 10 mm/s at $t = 80$ s and 100 s

For the low velocity case with a 1 mm/s liquid inlet velocity, the flow field demonstrates a clear time-dependent evolution, progressing from an initial developing phase to a stable, steady state. At 5 seconds, the fluid begins to accelerate as it approaches the heated block, and a small wake region starts to form downstream, with the overall velocity magnitude remaining low. By 20 seconds, this flow pattern becomes more pronounced, as the acceleration around the block intensifies and the wake region grows larger and more defined, although it still represents a zone of reduced momentum. The flow field then appears to reach a near-steady state at 80 seconds, exhibiting a stable acceleration and a well-established wake. Finally, at 100 seconds, the velocity contours show a pattern that is nearly identical to that at 80 seconds, indicating that the fluid dynamics for this specific low velocity have fully stabilized.

For the high velocity case, the flow field develops almost instantly due to the higher inlet momentum. At just 5 seconds, the flow is already highly developed, with a distinct high-velocity region clearly visible in the constricted gap around the heated block, and a significant wake region has already formed downstream. By 20 seconds, the velocity field is very well-established and stable, with velocity magnitudes an order of magnitude higher

than the low velocity case. This high momentum flow dominates the fluid dynamics, and the flow field reaches a steady state well before 80 seconds, as shown by the consistent pattern of high velocity around the block and a well-defined wake that persists through 100 seconds. This vigorous flow is the primary driving force for highly effective convective heat transfer, leading to a much more efficient removal of heat from the block compared to the low velocity case.

5.4 Effect of Geometry on Pressure

The pressure difference between the upstream (high-pressure) and downstream (low-pressure) sides of the heated block is the primary source of pressure drag. The contours clearly show that this pressure difference is much greater for the 10 mm/s flow, which means the block experiences a significantly higher drag force at this velocity.

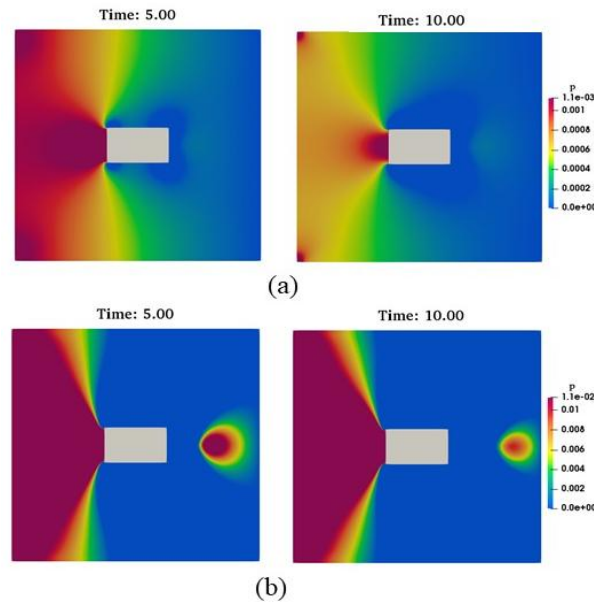


Figure 0.8: Transient pressure contours for fluid flow around a heated block, shown for inlet velocities of 1 mm/s and 10 mm/s at $t=5$ s and 10 s.

In the case of low velocity (1 mm/s), the pressure field exhibits a distinct and steady pattern. Five seconds has already shown the development of two unique pressure zones: a lower-pressure zone forms in the downstream wake, and a high-pressure zone arises on the upstream face of the heated block because of the fluid's stagnation. The block's pressure drag is directly caused by this pressure differential. The basic pattern has not altered by 10

seconds, while the pressure field has changed. The pressure contours are also comparatively symmetrical, with the low-pressure wake region being limited.

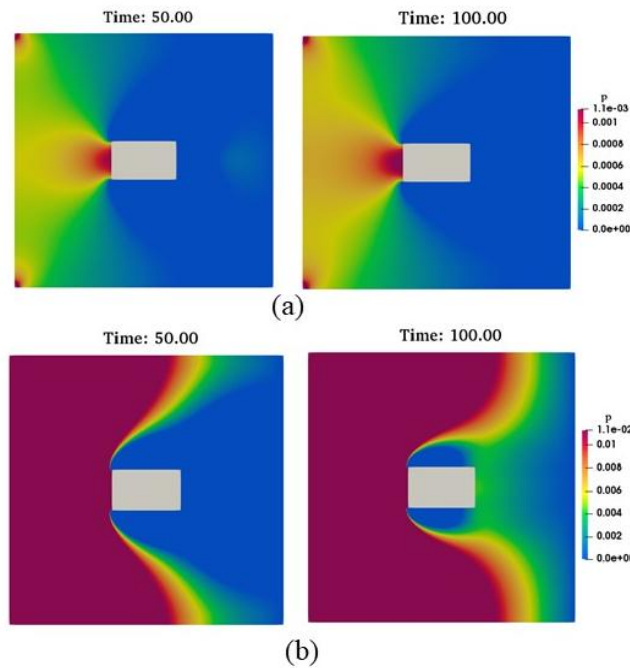


Figure 0.9: Transient pressure contours for fluid flow around a heated block, shown for inlet velocities of 1 mm/s and 10 mm/s at $t=50$ s and 100 s.

High Velocity (10 mm/s) $t = 5$ s, due to the higher fluid momentum, the pressure field develops almost instantly and is much more pronounced than in the low velocity case. The high-pressure region on the front face of the block is significantly larger and more intense. The low-pressure wake region is also much more distinct and elongated. Because of the increased fluid momentum in the high velocity case of 10 mm/s, the pressure field forms almost immediately and exhibits a considerably more noticeable pattern than in the low velocity case. At 5 seconds, the low-pressure wake region is already noticeable and elongated, and the high-pressure region on the heated block's front face is noticeably bigger and more intense. The square relationship between velocity and dynamic pressure directly results in pressure magnitudes that are an order of magnitude larger. This high momentum dominates the flow, and early in the simulation, the pressure field is well-established.

6. Conclusion and Future Prospects

6.1 Conclusion

This study makes use of the conjugate heat transfer approach with great accuracy in solving the heat transfer mechanism. This technique provides a robust and physically consistent framework for analysing conjugate heat transfer problems, allowing for a smooth transition from lower to higher velocity flow regimes. The behaviour of the fluid and thermal fields with varying flow rates, particularly focusing on the effects of velocity on cooling efficiency, temperature distribution, and pressure characteristics, is thoroughly investigated. The inlet fluid velocity within the channel significantly influences the system's thermal state, with higher velocities leading to enhanced convective cooling and lower peak temperatures. At a low inlet velocity of 1 mm/s, the flow is characterized by less efficient heat removal. The fluid spends more time in contact with the heated block, resulting in a pronounced and intense thermal plume that is confined to a relatively small downstream region. The flow field, while showing acceleration around the obstacle, exhibits low momentum, leading to a smaller pressure difference across the block and a low-velocity wake. The system's thermal state at this velocity is dominated by the slow convective transport of energy, resulting in a higher overall temperature. Conversely, at a high inlet velocity of 10 mm/s, the flow is dominated by a strong forced convection. The high fluid momentum leads to a much more effective cooling process, where the heat plume is significantly elongated and less concentrated, indicating rapid heat transport away from the source. The velocity profiles show a much more pronounced acceleration around the block, and the pressure contours reveal a significantly larger pressure difference between the upstream and downstream faces, resulting in a greater pressure drag. The flow field develops almost instantly and reaches a steady state much faster than the low velocity case. The drag force experienced by the heated block varies significantly with the flow rate, with the high-velocity case exhibiting a much larger pressure difference between the upstream and downstream faces, which directly contributes to a greater pressure drag. The transient analysis reveals that the flow field for the higher velocity case reaches a steady state much faster, with the high momentum of the fluid dominating the flow patterns early in the simulation. These findings highlight the critical role of forced convection in thermal management applications.

6.2 Future Prospects

This two-dimensional conjugate heat transfer problem's fundamental analysis provides several research directions. Investigating more realistic flow phenomena, like turbulent flow and intricate thermal boundary layers, which are essential for real-world applications, would be possible by extending the simulation to a three-dimensional domain. Additionally, adding sophisticated physics like temperature-dependent fluid characteristics or time-varying heat loads would improve the model's accuracy and represent a greater variety of real-world behaviors. To determine the best configurations for maximum heat dissipation, optimization studies could also be conducted, investigating different geometric modifications to the heated block or putting active cooling tactics into practice. The goal of these future opportunities is to transform the existing basic knowledge into a more thorough and immediately useful foundation for challenging thermal management issues.

References

- [1] A. Alkhazaleh, F. Alnaimat, and B. Mathew, “Fluid flow and heat transfer behavior of a liquid based MEMS heat sink having wavy microchannels integrating circular pin-fins,” **Int. J. Thermofluids**, vol. 20, pp. 2–3, Nov. 2023, doi: 10.1016/j.ijft.2023.100480.,
- [2] J. M. Kim, S. G. Lee, and C. Kim, “Numerical simulations of particle migration in suspension flows: Frame-invariant formulation of curvature-induced migration,” **J. Non-Newtonian Fluid Mech.**, vol. 150, no. 2–3, p. 6, Apr. 2008, doi: 10.1016/j.jnnfm.2007.10.012.
- [3] N. Fathi, M. Pourghasemi, S. S. Aleyasin, L. Savoldi, and S. Rodriguez, “On conjugate heat transfer in microchannel heat sinks,” **Int. J. Thermofluids**, vol. 22, pp. 7–10, May 2024, doi: 10.1016/j.ijft.2024.100658.
- [4] Y. Yang et al., “Embedded microfluidic cooling with compact double H type manifold microchannels for large-area high-power chips,” **Int. J. Heat Mass Transf.**, vol. 197, pp. 10–12, Nov. 2022, doi: 10.1016/j.ijheatmasstransfer.2022.123340.